



Original Research

Enhanced utilization efficiency of peroxymonosulfate via water vortex-driven piezo-activation for removing organic contaminants from water

Chuan Yu ^a, Jie He ^a, Shenyu Lan ^a, Wanqian Guo ^b, Mingshan Zhu ^{a, b, *}^a Guangdong Key Laboratory of Environmental Pollution and Health, School of Environment, Jinan University, Guangzhou, 511443, PR China^b State Key Laboratory of Urban Water Resource and Environment, Harbin Institute of Technology, Harbin, 150090, PR China

ARTICLE INFO

Article history:

Received 27 December 2021

Received in revised form

1 March 2022

Accepted 1 March 2022

Keywords:

Water vortex-driven

Peroxymonosulfate utilization

Piezoelectric activation

Organic contaminants

Few-odd-layered MoS₂

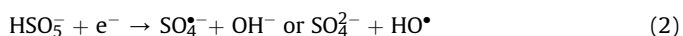
ABSTRACT

The efficient activation and utilization of peroxymonosulfate (PMS) in PMS-based advanced oxidation processes is a high-priority target for the removal of organic contaminants. This work introduces a water vortex-driven piezoelectric effect from few-odd-layered MoS₂ into the PMS activation to remove benzotriazole (BTR) and other organic contaminants from the water. Approximately 91.1% of BTR can be removed by the MoS₂ piezo-activated PMS process with a reaction rate constant of 0.428 min⁻¹, which is 2.09 times faster than the sum of the individual MoS₂, water vortex, and piezocatalysis rates. Meanwhile, the PMS utilization efficiency reached 0.0147 in the water vortex-driven piezo-activation system, which is 3.97 times that of the sum from the vortex/PMS and MoS₂/PMS systems. These results demonstrate that the presence of MoS₂ under a water vortex can trigger a piezoelectric potential and generate abundant free electrons to activate PMS to generate various active species for degradation of organic contaminants.

© 2022 The Authors. Published by Elsevier B.V. on behalf of Chinese Society for Environmental Sciences, Harbin Institute of Technology, Chinese Research Academy of Environmental Sciences. This is an open access article under the CC BY-NC-ND license (<http://creativecommons.org/licenses/by-nc-nd/4.0/>).

1. Introduction

Peroxymonosulfate (PMS)-based advanced oxidation processes (AOPs) have aroused immense interest for *in-situ* chemical oxidation for remediation of contaminated wastewater [1–5]. For this application, PMS, with its asymmetric structure (HO–O–SO₃⁻), needs to be activated by the input of energy or by the electron transfers indicated in Eqs. (1) and (2) to break the superoxide O–O bond. This then generates strong reactive oxygen species (ROS) to oxidize organic contaminants in water [6–11]. Thus, the decomposition and utilization efficiency of PMS are extremely important factors to be considered in water treatment applications.



* Corresponding author. Guangdong Key Laboratory of Environmental Pollution and Health, School of Environment, Jinan University, Guangzhou, 511443, PR China. E-mail address: zhumingshan@jnu.edu.cn (M. Zhu).

A wide variety of strategies have been employed for PMS activation, such as the use of metal ions, ultraviolet (UV), heating, or ultrasonication (US) [8,12–16]. However, the introduction of transition metals not only consumes a large amount of chemicals but also brings some drawbacks with regards secondary pollution from the leaching of metal ions or more difficult recovery of the catalyst. Moreover, UV, heating, or US will cause a high energy consumption [17], thus limiting their application for industrial scale wastewater treatments (Scheme 1). Therefore, it is imperative to find an environmentally friendly, simple yet effective method for PMS activation to enhance PMS utilization efficiency.

The piezoelectric effect is gaining much attention as a physical phenomenon that converts mechanical vibrations into electrical energy [18,19]. In this process, an external mechanical force induces the deformation and polarization of the piezoelectric material to form a piezo-potential to drive the transfer and migration of intrinsic free electrons [20]. The piezoelectric effect has been applied for the elimination of contaminants and the activation of PMS [21–24]. However, most of these applications required external energy from ultrasonic vibration with a relatively high frequency (kHz) to trigger deformation of the piezoelectric materials, which also caused high energy consumption and limited their

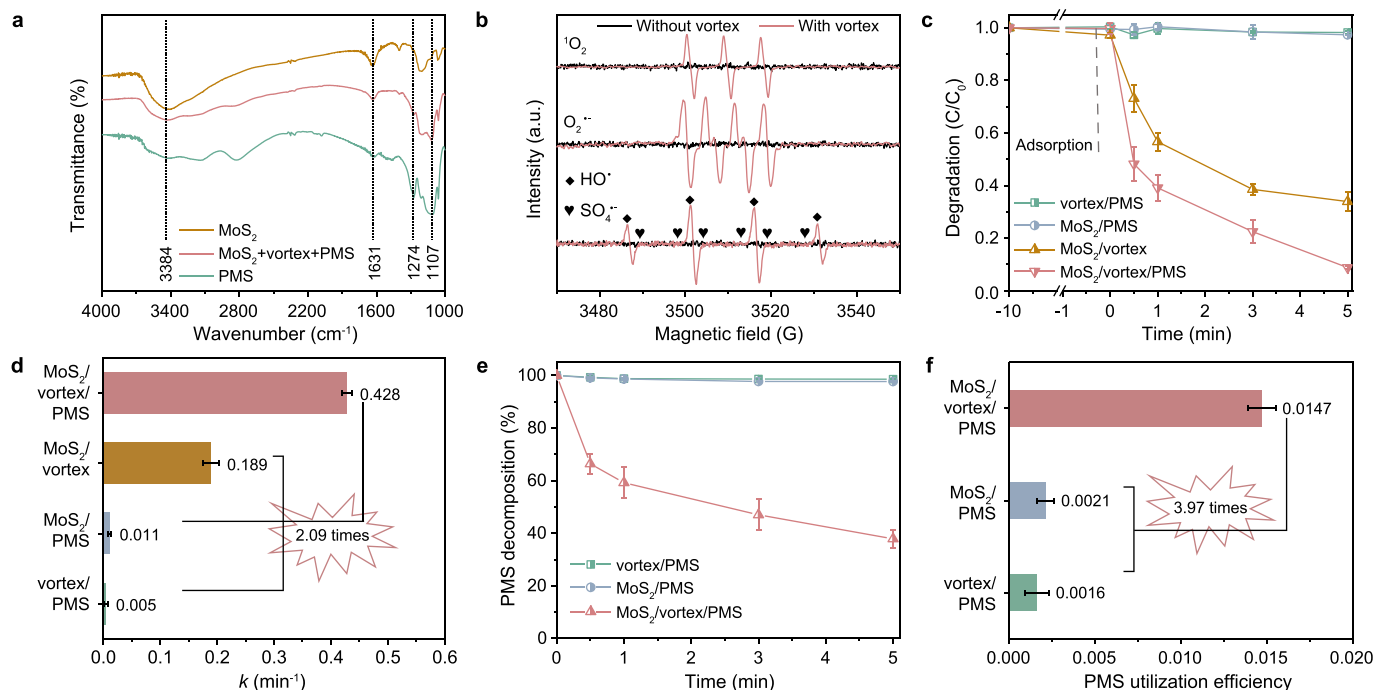


Fig. 1. FTIR spectra (a), EPR spectra (b) in the MoS₂/vortex/PMS system. (c), BTR degradation curves. (d), pseudo-first order kinetics. (e), PMS decomposition. (f), PMS utilization efficiency. (Experiment conditions: [MoS₂]₀ = 0.5 g L⁻¹, [PMS]₀ = 0.5 g L⁻¹, [BTR]₀ = 5 mg L⁻¹, stirring speed = 1600 rpm, and T = 25 °C).

the PMS decomposition and utilization efficiency were evaluated by measuring the PMS concentration and calculating the reaction stoichiometric efficiency. Fig. 1e shows that the PMS decomposition efficiencies reached 62.11% in MoS₂/vortex/PMS, 2.31% in MoS₂/PMS, and 1.41% in the vortex/PMS system. More PMS molecules were decomposed in the MoS₂ piezocatalytic system, indicating the O–O bond of PMS was broken through electron transfers from the piezo-process. Moreover, the PMS utilization efficiency of MoS₂/vortex/PMS reached 0.0147, which was 3.97 times greater than the sum of the vortex/PMS (0.0016) and MoS₂/PMS (0.0021) systems (Fig. 1f). This is because the external hydromechanical energy from the vortex triggered the piezo-response of MoS₂ to generate more electrons for PMS activation to then produce various active species. This showed a competitive PMS utilization efficiency than a previous study [34].

The influences of MoS₂ and PMS dosage in the MoS₂ piezo-activated PMS process were further studied. From Fig. S6a, the BTR degradation efficiency gradually increased with an increase in MoS₂ content. Similarly, an increase in the PMS dosage from 0 to 0.5 g L⁻¹ also significantly promoted BTR degradation, but the elevation was insignificant when the PMS dosage was greater than 0.5 g L⁻¹ because of the self-consumption of SO₄^{•-} by excessive PMS (Fig. S6b) [35]. These results suggest that only a suitable dosage of catalyst and PMS are beneficial to the reactive species generation and PMS utilization.

Moreover, the mineralization degree of BTR was determined using total organic carbon (TOC) analysis. From Fig. S7, approximately 24% of TOC was removed within 60 min in the MoS₂/vortex/PMS system, suggesting that some organic intermediates were generated during the process.

3.3. Effects of different operational parameters

The effects of different operational parameters on pollution degradation were further evaluated in the piezo-activated PMS process, including scavenger molecule concentration; stirring speed;

catalysts, pollutant, and ion types; water matrixes; and the catalyst reusability. To elucidate the contribution of each ROS on the BTR degradation in the MoS₂/vortex/PMS system, experiments were conducted on the existence of different radical scavengers, including AgNO₃ (scavenger of e⁻), EDTA-2Na (scavenger of h⁺), methanol (MeOH, scavenger of HO[•]/SO₄^{•-}), SOD (scavenger of O₂^{•-}), tert-butanol (TBA, scavenger of HO[•]), and histidine (His, scavenger of ¹O₂) [36]. From Fig. S8, the introduction of His provided a dramatic inhibitory effect, and the BTR degradation efficiency decreased from 91.1% to 4.5%. With the addition of AgNO₃, EDTA-2Na, MeOH, TBA, and SOD, the BTR removal efficiencies slightly reduced from 91.1% to 74.4%, 70.3%, 71.1%, 83.5%, and 81.9%, respectively. The results indicated that ¹O₂ played a dominant role in BTR degradation while other reactive species made a minor contribution. In light of the generation of HO[•], SO₄^{•-}, and O₂^{•-} and ¹O₂ during PMS activation by the MoS₂/vortex system, their contributions to the catalytic degradation of BTR were quantified (see Text S5 and Fig. S9) [37,38]. From Fig. 2a, the contributions of HO[•] and SO₄^{•-}, O₂^{•-} and ¹O₂ were calculated to be 44.9%, 22.9%, and 97.5%, respectively.

Furthermore, piezoelectricity is known to be dependent on the applied stress employed. From Fig. 2b, the BTR removal efficiency gradually increased with the increase in magnetic stirring speed. This is because faster stirring can provide a stronger vortex to drive MoS₂ to produce a stronger piezo-potential. It is beneficial for the harvest of hydromechanical vibration to induce catalytic redox reactions, thereby facilitating PMS activation to degrade BTR.

Moreover, a comparison of PMS utilization efficiency was carried out among as-prepared MoS₂, BaTiO₃, and commercial MoS₂. BaTiO₃ and non-piezoelectric commercial MoS₂ showed negligible BTR degradation efficiencies and limited PMS utilization efficiencies (Fig. 2c and Fig. S10). This is because the weak external hydromechanical energy from the vortex was not able to motivate the piezoelectric response of BaTiO₃, and the non-piezoelectric commercial MoS₂ had no piezoelectric property, therefore both of these cannot generate a piezoelectric effect to activate the PMS under a water vortex.

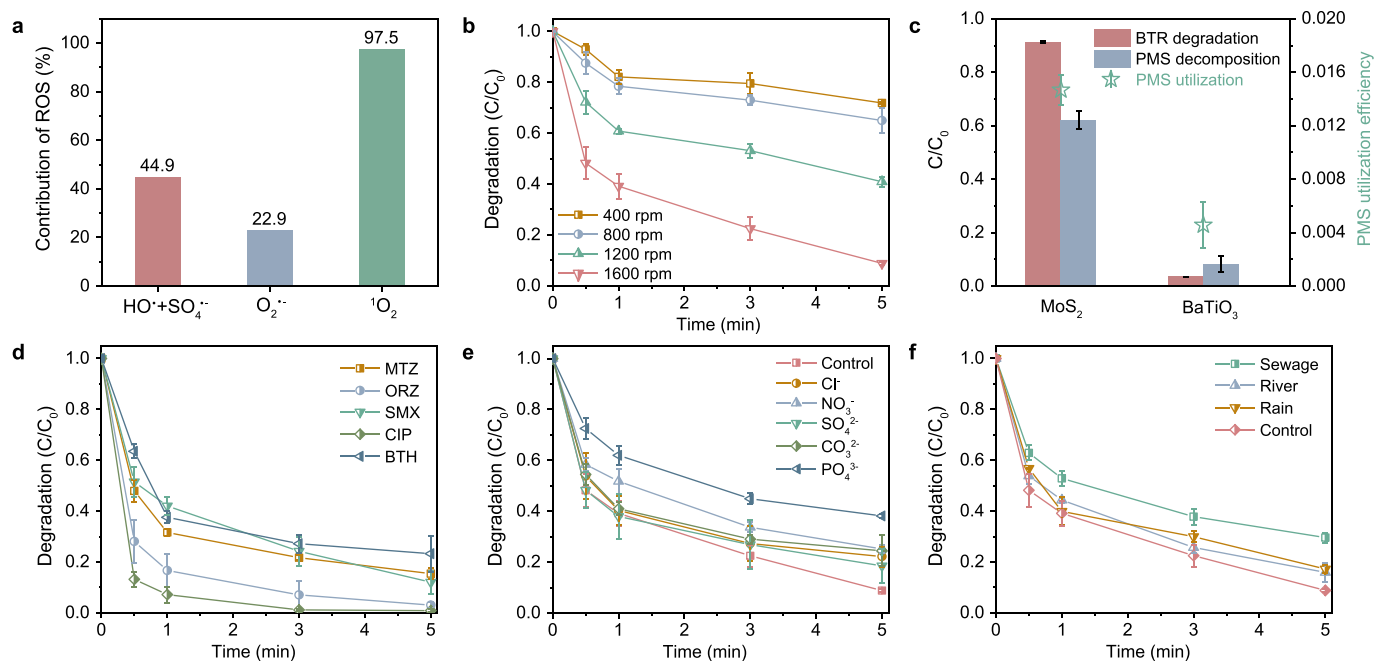


Fig. 2. a, Contribution of ROSs on BTR removal in MoS₂/vortex/PMS process. Effects of the magnetic stirring speed (b), different catalysts (c), different pollutants (d), co-existing anions (e), and water matrices on pollutant removal (f) in MoS₂/vortex/PMS process. (Experiment conditions: [catalyst]₀ = 0.5 g L⁻¹, [PMS]₀ = 0.5 g L⁻¹, [pollutants]₀ = 5 mg L⁻¹, [anions]₀ = 5 mmol L⁻¹, stirring speed = 400–1600 rpm and T = 25 °C).

In addition to BTR, other various organic pollutants, including ciprofloxacin (CIP), ornidazole (ORZ), sulfamethoxazole (SMX), metronidazole (MTZ), and benzothiazole (BTH) were also investigated. As shown in Fig. 2d, the removal efficiency reached, respectively, 99.2%, 97.1%, 88.3%, 85.6%, and 78.9% in the water vortex-driven piezo-activation of the PMS system. These results solidly confirm the excellent organic contaminants treatment performance in the present MoS₂/vortex/PMS system.

As common factors widely existing in actual wastewater, Cl⁻, NO₃⁻, CO₃²⁻, SO₄²⁻, and PO₄³⁻ were selected to investigate their influence on BTR degradation (Fig. 2e). The BTR removal efficiency slightly decreased from 91.1% to 78.4%, 75.3%, 76.1%, and 81.5% in the presence of Cl⁻, NO₃⁻, CO₃²⁻, and SO₄²⁻ anions, respectively, but dropped to 62.2% in the presence of PO₄³⁻. This may be because the PO₄³⁻ competed with BTR to consume the ROS [39].

In complexed water matrices, the BTR removal ratio was slightly decreased, being 70.4%, 81.1%, and 61.6% in rain, river, and sewage, respectively (Fig. 2f). This is because some amounts of organic substances existed in these practical water media (Table S1), and these may form a competitive relationship with BTR for ROS. In addition, the used MoS₂ was employed to further study the recycling performance for BTR degradation in the MoS₂/vortex/PMS reaction system (Fig. S11). A comparative BTR degradation efficiency was observed after 4 cycles (85.3%), demonstrating the excellent stability and reusability. Moreover, the morphology of the used MoS₂ was explored by TEM (Fig. S12a) and HRTEM (Fig. S12b), showing a similar structure to the fresh MoS₂ and indicating the stability of the MoS₂.

Generally, the average concentration of BTR is detected with 10 µg L⁻¹ in a natural water body, and the concentration can reach up to 1.1 mg L⁻¹ in the groundwater below a deicing pad, at a regeneration plant and snow disposal site [40–42]. Moreover, in wastewater treatment plants, the concentrations of pollutants are generally high, where the unit of concentrations of pollutants can reach from µg L⁻¹ to mg L⁻¹. Accordingly, different initial concentrations of BTR were further studied. From Fig. S13, the degradation

efficiency of BTR was almost 100% at the initial concentration of 1 mg L⁻¹, 96.9% at 5 mg L⁻¹, 85.3% at 10 mg L⁻¹, and 76.2% at 20 mg L⁻¹ within 30 min. However, the BTR degradation efficiency was only 54.1% at an initial concentration of 50 mg L⁻¹ within 30 min in the MoS₂/vortex/PMS system. The higher initial BTR concentration resulted in a decrease in the BTR degradation efficiency, which was due to the increase in BTR molecules competing with each other for the active species to lower the whole removal efficiency.

In addition, the pH of the point of zero charge (pHpzc) of the MoS₂ was measured to be approximately 2.8 using a Malvern Zetasizer Nano ZSE (Fig. S14a). The influence of the initial pH on the BTR degradation was studied. From Fig. S14b, the BTR degradation was significantly inhibited under alkaline conditions, and slightly enhanced in acidic solution. A detailed discussion on this topic is provided in the supplementary materials.

3.4. BTR degradation pathways and toxicity assessment

The Fukui function distribution was calculated to predict the active sites for ROS during the attack of the BTR molecules. An optimized BTR model is presented in Fig. 3a and the Fukui function values of f^0 are shown in Fig. 3b and Table S2. The 3C and 6C atoms, with higher f^0 values, were more susceptible to be nucleophilically attacked, while the 7N and 9N atoms, with lower f^0 values, were more easily electrophilically attacked [43]. Based on the theoretical calculation of the Fukui function and the liquid chromatography quadrupole time-of-flight tandem mass spectrometry (LC-TOF-MS) data, possible pathways for the BTR degradation were proposed (Fig. 3c). In terms of pathway I, the hydroxylation of the aromatic ring first occurred at 3C and 6C after being attacked by a hydroxide radical, and the aromatic ring was further opened to generate product of E ($m/z = 127$), F ($m/z = 127$), and G ($m/z = 127$), then the product O ($m/z = 74$) and P ($m/z = 157$) was produced via further oxidation and ring opening of J, K, L, and M [44]. In pathway II, the triazole ring was opened by the ROS, hydroxylated, then had the

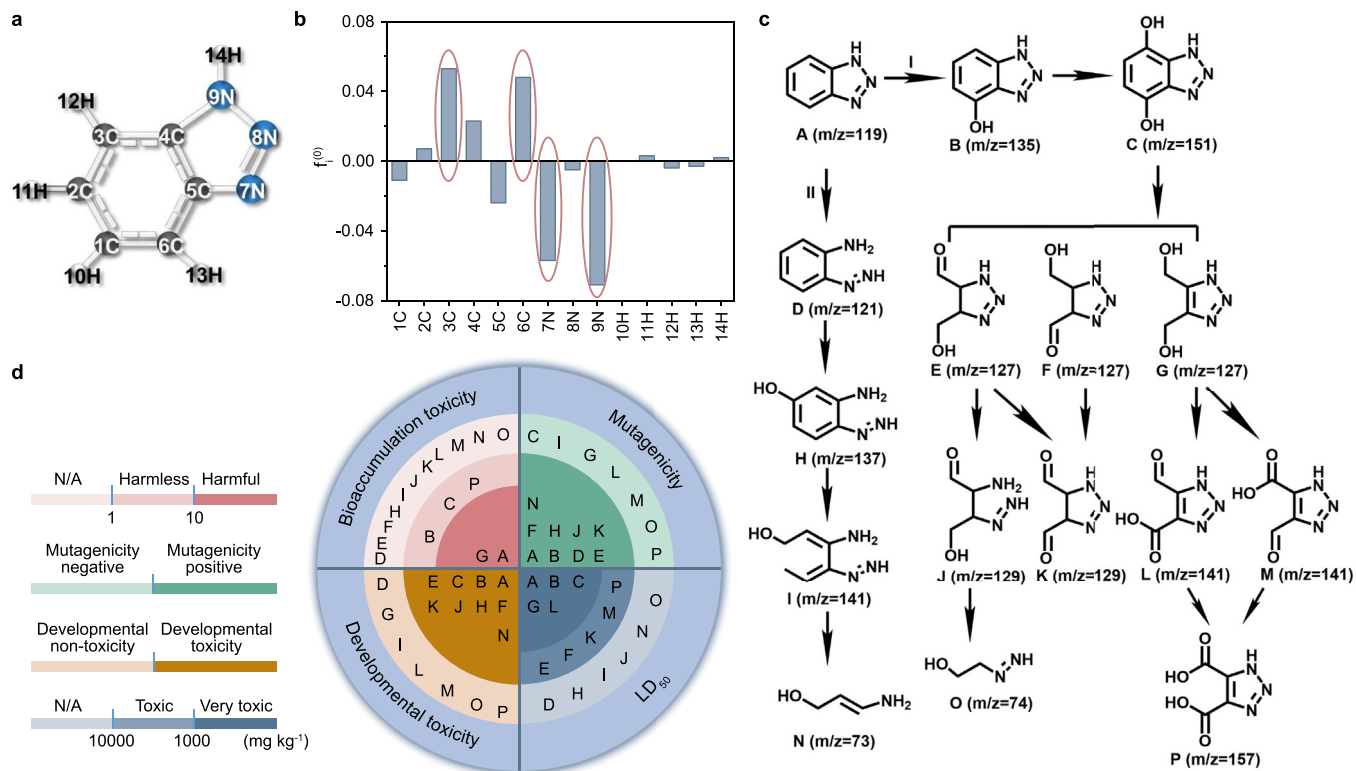
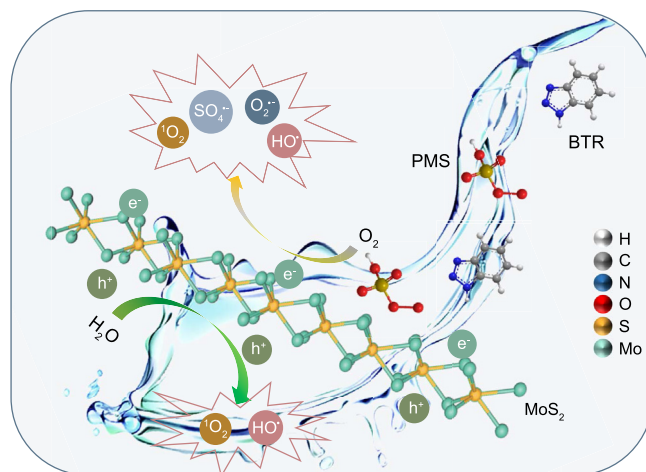
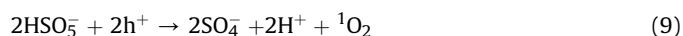
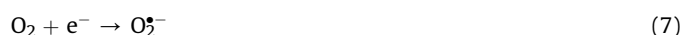


Fig. 3. a, BTR molecular structure. b, DFT calculation of BTR. c, Proposed degradation pathways of BTR. d, Acute toxicity, developmental toxicity, mutagenicity and bioaccumulation toxicity of BTR and its degradation products.

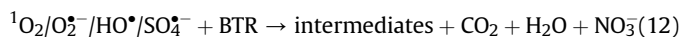
C–C bond cleaved to successively form D, H, I, and N [45–47].

Moreover, the acute toxicity of BTR and its intermediate degradation products were evaluated using the Toxicity Estimation Software Tool (T.E.S.T.) with a quantitative structure-activity relationship (QSAR) mathematical model including acute toxicity, developmental toxicity, mutagenicity, and bioaccumulation toxicity (Text S6). From Fig. 3d and Table S3, the bioaccumulation toxicity of the degradation intermediate products was lower than that of BTR (except for G). From the results of the developmental toxicity and mutagenicity, seven kinds of intermediate in the BTR degradation would be mutagenic negative and developmentally nontoxic, while the parent compound was mutagenic positive and developmentally toxic. Moreover, compared with the LD_{50} of BTR (326.3 mg kg^{-1}), the toxicity of its products are clearly reduced. These results indicated that the bioaccumulation toxicity, mutagenicity, developmental toxicity, and acute toxicity of BTR can be effectively decreased and weakened.

Based on the above discussion, a mechanism diagram and the corresponding ROS chain reactions for BTR degradation by MoS_2 piezoelectric-activated PMS were proposed (Eq. (3)–(12) and Scheme 2). In this process, MoS_2 was triggered by the external hydro-mechanical energy from the water vortex to produce a piezoelectric potential to drive the transfer of free charges. These free electrons activated PMS to produce various reactive species, including HO^\bullet , $\text{SO}_4^{\bullet-}$, $\text{O}_2^{\bullet-}$, and $^1\text{O}_2$. Then, these powerful reactive species fragmented the BTR molecules into different intermediates, small molecule compounds, and CO_2 , H_2O and NO_3^- [21,48–52].



Scheme 2. Mechanism of MoS_2 piezoelectric activated PMS for BTR degradation.



4. Conclusions

The low frequency of hydromechanical energy from a water vortex works on piezoelectric MoS₂ to generate piezoelectric potential induced charges, which further effectively activate PMS for organic contaminants degradation. Upon the assistance of MoS₂ in this water-vortex-driven piezo-activation PMS process, significant enhancements to organic contaminants degradation and PMS utilization were achieved which were greater than the sum of the contributions from individual MoS₂-, water vortex-, and piezocatalysis-PMS activation. The enhancements were attributed to the piezo-potential from MoS₂ promoting the transfer of charges, thus more electrons participated in the activation reaction of PMS to generate powerful reactive oxygen species for organic contaminants degradation. Different reactive oxygen species, e.g., HO[•], SO₄^{•-}, O₂^{•-}, and ¹O₂, were detected in the system while ¹O₂ was the dominant ROS. Finally, 15 less-harmful intermediates from BTR degradation were identified and produced through two possible reaction pathways. This investigation provides a promising way to enhance the utilization efficiency of PMS as well as the decontamination of organic pollutants by using an environmentally friendly water vortex in environmental remediation.

Declaration of competing interest

The authors declare no competing financial interest.

Acknowledgments

This work is financially supported by Open Project of State Key Laboratory of Urban Water Resource and Environment, Harbin Institute of Technology (ESK202102), the Guangdong Basic and Applied Basic Research Foundation (2020B1515020038), and National Natural Science Foundation of China (22006052).

Appendix A. Supplementary data

Supplementary data to this article can be found online at <https://doi.org/10.1016/j.ese.2022.100165>.

References

- [1] M.Y. Kilic, W.H. Abdelraheem, X. He, K. Kestioglu, D.D. Dionysiou, Photochemical treatment of tyrosol, a model phenolic compound present in olive mill wastewater, by hydroxyl and sulfate radical-based advanced oxidation processes (AOPs), *J. Hazard. Mater.* 367 (2019) 734–742.
- [2] C. Nie, Z. Dai, W. Liu, X. Duan, C. Wang, B. Lai, Z. Ao, S. Wang, T. An, Criteria of active sites in nonradical persulfate activation process from integrated experimental and theoretical investigations: boron–nitrogen-co-doped nanocarbon-mediated peroxydisulfate activation as an example, *Environ. Sci. Nano* 7 (2020) 1899–1911.
- [3] S. Zhao, C. Chen, J. Ding, S. Yang, Y. Zang, X. Qin, X. Gao, Z. Song, N. Ren, Fabrication of AQ2S/GR composite photosensitizer for the simulated solar light-driven degradation of sulfapyridine, *Environ. Sci. Ecotechnol.* 8 (2021) 100111.
- [4] A. Hassani, S. Krishnan, J. Scaria, P. Eghbali, P.V. Nidheesh, Z-scheme photocatalysts for visible-light-driven pollutants degradation: a review on recent advancements, *Curr. Opin. Solid State Mater. Sci.* 25 (2021) 100941.
- [5] A. Hassani, P. Eghbali, B. Kakavandi, K.Y.A. Lin, F. Ghanbari, Acetaminophen removal from aqueous solutions through peroxymonosulfate activation by CoFe₂O₄/mpg-C₃N₄ nanocomposite: insight into the performance and degradation kinetics, *Environ. Technol. Inno.* 20 (2020) 101127.
- [6] D. Yu, J. He, T. Xie, Q. Xu, Q. Zhu, J. Yang, J. An, F. Ye, J. Wang, B. Xiang, New insights into Sr–O bonds enhances Co/Fe catalytic activity in SrCoFe perovskite for boosted peroxymonosulfate activation, *Chem. Eng. J.* 426 (2021) 131525.
- [7] Y. Wu, X. Chen, Y. Han, D. Yue, X. Cao, Y. Zhao, X. Qian, Highly efficient utilization of nano-Fe(0) embedded in mesoporous carbon for activation of peroxydisulfate, *Environ. Sci. Technol.* 53 (2019) 9081–9090.
- [8] S. Lan, Y. Chen, L. Zeng, H. Ji, W. Liu, M. Zhu, Piezo-activation of peroxymonosulfate for benzothiazole removal in water, *J. Hazard. Mater.* 393 (2020) 122448.
- [9] S. Madihi-Bidgoli, S. Asadnezhad, A. Yaghoot-Nezhad, A. Hassani, Azurobine degradation using Fe₂O₃@multi-walled carbon nanotube activated peroxymonosulfate (PMS) under UVA-LED irradiation: performance, mechanism and environmental application, *J. Environ. Chem. Eng.* 9 (2021) 106660.
- [10] W. Tian, J. Lin, H. Zhang, X. Duan, H. Wang, H. Sun, S. Wang, Kinetics and mechanism of synergistic adsorption and persulfate activation by N-doped porous carbon for antibiotics removals in single and binary solutions, *J. Hazard. Mater.* 423 (2022) 127083.
- [11] Y. Yu, N. Li, X. Lu, B. Yan, G. Chen, Y. Wang, X. Duan, Z. Cheng, S. Wang, Co/N co-doped carbonized wood sponge with 3D porous framework for efficient peroxymonosulfate activation: performance and internal mechanism, *J. Hazard. Mater.* 421 (2022) 126735.
- [12] S. He, R. Yin, Y. Chen, T. Lai, W. Guo, L. Zeng, M. Zhu, Consolidated 3D Co₃Mn layered double hydroxide aerogel for photo-assisted peroxymonosulfate activation in metronidazole degradation, *Chem. Eng. J.* 423 (2021) 130172.
- [13] Y. Lee, S. Lee, M. Cui, Y. Ren, B. Park, J. Ma, Z. Han, J. Khim, Activation of peroxydisulfate and peroxymonosulfate by ultrasound with different frequencies: impact on ibuprofen removal efficient, cost estimation and energy analysis, *Chem. Eng. J.* 413 (2021) 127487.
- [14] S. Lan, C. Yu, F. Sun, Y. Chen, D. Chen, W. Mai, M. Zhu, Tuning piezoelectric driven photocatalysis by La-doped magnetic BiFeO₃-based multiferroics for water purification, *Nano Energy* 93 (2022) 106792.
- [15] X. Hu, Y. Ye, Y. Chen, M. Liu, W. Zhang, M. Zhu, The synergistic interactions of reaction parameters in heterogeneous peroxymonosulfate oxidation: reaction kinetic and catalytic mechanism, *J. Hazard. Mater.* 421 (2022) 126841.
- [16] F. Ghanbari, Q. Wang, A. Hassani, S. Waclawek, J. Rodriguez-Chueca, K.A. Lin, Electrochemical activation of peroxides for treatment of contaminated water with landfill leachate: efficacy, toxicity and biodegradability evaluation, *Chemosphere* 279 (2021) 130610.
- [17] H. Ding, Y. Zhu, Y. Wu, J. Zhang, H. Deng, H. Zheng, Z. Liu, C. Zhao, In situ eegeneration of phenol-saturated activated carbon fiber by an electro-peroxymonosulfate process, *Environ. Sci. Technol.* 54 (2020) 10944–10953.
- [18] S. Lan, C. Yu, E. Wu, M. Zhu, D.D. Dionysiou, Self-powered water flow-triggered piezocatalytic generation of reactive oxygen species for water purification in simulated water drainage, *ACS ES&T Engg.* 2 (2022) 101–109.
- [19] Y.T. Lin, S.N. Lai, J.M. Wu, Simultaneous piezoelectrocatalytic hydrogen-evolution and degradation of water pollutants by quartz microrods@few-layered MoS₂ hierarchical heterostructures, *Adv. Mater.* 32 (2020) 2002875.
- [20] T.M. Chou, S.W. Chan, Y.J. Lin, P.K. Yang, C.C. Liu, Y.J. Lin, J.M. Wu, J.T. Lee, Z.H. Lin, A highly efficient Au–MoS₂ nanocatalyst for tunable piezocatalytic and photocatalytic water disinfection, *Nano Energy* 57 (2019) 14–21.
- [21] Y. Chen, S. Lan, M. Zhu, Construction of piezoelectric BaTiO₃/MoS₂ heterojunction for boosting piezo-activation of peroxymonosulfate, *Chin. Chem. Lett.* 32 (2021) 2052–2056.
- [22] S. Liu, B. Jing, C. Nie, Z. Ao, X. Duan, B. Lai, Y. Shao, S. Wang, T. An, Piezoelectric activation of peroxymonosulfate by MoS₂ nanoflowers for the enhanced degradation of aqueous organic pollutants, *Environ. Sci. Nano* 8 (2021) 784–794.
- [23] S. Lan, B. Jing, C. Yu, D. Yan, Z. Li, Z. Ao, M. Zhu, Protrudent iron single-atom accelerated interfacial piezoelectric polarization for self-powered water motion triggered Fenton-like reaction, *Small* 18 (2022) 2105279.
- [24] M. Zhu, S. Li, H. Zhang, J. Gao, K.W. Kwok, Y. Jia, L.B. Kong, W. Zhou, B. Peng, Diffused phase transition boosted dye degradation with Ba(Zr_xTi_{1-x})O₃ solid solutions through piezoelectric effect, *Nano Energy* 89 (2021) 106474.
- [25] X. Liu, L. Shen, W. Xu, W. Kang, D. Yang, J. Li, S. Ge, H. Liu, Low frequency hydromechanics-driven generation of superoxide radicals via optimized piezotronic effect for water disinfection, *Nano Energy* 88 (2021) 106290.
- [26] Y. Su, L. Zhang, W. Wang, X. Li, Y. Zhang, D. Shao, Enhanced H₂ evolution based on ultrasound-assisted piezo-catalysis of modified MoS₂, *J. Mater. Chem. A* 6 (2018) 11909–11915.
- [27] J.M. Wu, W.E. Chang, Y.T. Chang, C.K. Chang, Piezo-catalytic effect on the enhancement of the ultra-high degradation activity in the dark by single- and few layers MoS₂ nanoflowers, *Adv. Mater.* 28 (2016) 3718–3725.
- [28] C.Y. Tu, J.M. Wu, Localized surface plasmon resonance coupling with piezophototronic effect for enhancing hydrogen evolution reaction with Au@MoS₂ nanoflowers, *Nano Energy* 87 (2021) 106131.
- [29] C. Li, Y. Huang, X. Dong, Z. Sun, X. Duan, B. Ren, S. Zheng, D.D. Dionysiou, *Appl. Catal. B Environ.* 247 (2019) 10–23.
- [30] T. Zhang, H. Zhu, J.P. Croue, Production of sulfate radical from peroxymonosulfate induced by a magnetically separable CuFe₂O₄ spinel in water: efficiency, stability, and mechanism, *Environ. Sci. Technol.* 47 (2013) 2784–2791.
- [31] K. Zhang, K.M. Parker, Halogen radical oxidants in natural and engineered aquatic systems, *Environ. Sci. Technol.* 52 (2018) 9579–9594.
- [32] A. Wang, Z. Hua, C. Chen, W. Wei, B. Huang, S. Hou, X. Li, J. Fang, Radical chemistry and PPCP degradation in the UV/peroxydisulfate process in the presence of chloride at freshwater levels, *Chem. Eng. J.* 426 (2021) 131276.
- [33] W. Wu, L. Wang, Y. Li, F. Zhang, L. Lin, S. Niu, D. Chenet, X. Zhang, Y. Hao, T.F. Heinz, J. Hone, Z. L. Piezoelectricity of single-atomic-layer MoS₂ for energy

- conversion and piezotronics, Wang, Nature 514 (2014) 470–474.
- [34] J. Ali, L. Wenli, A. Shahzad, J. Iftikhar, G.G. Aregay, I.I. Shahib, Z. Elkhilfi, Z. Chen, Z. Chen, Regulating the redox centers of Fe through the enrichment of Mo moiety for persulfate activation: a new strategy to achieve maximum persulfate utilization efficiency, Water Res. 181 (2020) 115862.
- [35] F. Liu, H. Zhou, Z. Pan, Y. Liu, G. Yao, Y. Guo, B. Lai, Degradation of sulfamethoxazole by cobalt-nickel powder composite catalyst coupled with peroxymonosulfate: performance, degradation pathways and mechanistic consideration, J. Hazard. Mater. 400 (2020) 123322.
- [36] W. Yu, F. Chen, Y. Wang, L. Zhao, Rapid evaluation of oxygen vacancies-enhanced photogeneration of the superoxide radical in nano-TiO₂ suspension, RSC Adv. 10 (2020) 29082–29089.
- [37] Y. Gao, Y. Zhu, T. Li, Z. Chen, Q. Jiang, Z. Zhao, X. Liang, C. Hu, Unraveling the high-activity origin of single-atom iron catalysts for organic pollutant oxidation via peroxymonosulfate activation, Environ. Sci. Technol. 55 (2021) 8318–8328.
- [38] N. Li, R. Li, X. Duan, B. Yan, W. Liu, Z. Cheng, G. Chen, L. Hou, S. Wang, Correlation of active sites to generated reactive species and degradation routes of organics in peroxymonosulfate activation by Co-loaded carbon, Environ. Sci. Technol. 55 (2021) 16163–16174.
- [39] M. Sui, L. Sheng, K. Lu, F. Tian, FeOOH catalytic ozonation of oxalic acid and the effect of phosphate binding on its catalytic activity, Appl. Catal. B Environ. 96 (2010) 94–100.
- [40] H. Janna, M.D. Scrimshaw, R.J. Williams, J. Churchley, J.P. Sumpter, From dishwasher to tap? Xenobiotic substances benzotriazole and tolyltriazole in the environment, Environ. Sci. Technol. 45 (2011) 3858–3864.
- [41] W. Giger, C. Schaffner, H.-P.E. Kohler, Benzotriazole and tolyltriazole as aquatic contaminants. 1. input and occurrence in rivers and lakes, Environ. Sci. Technol. 40 (2006) 7186–7192.
- [42] G.D. Breedveld, R. Roseth, M. Sparrevik, T. Hartnik, L.J. Hem, Persistence of the de-icing additive benzotriazole at an abandoned airport, Water Air Soil Pollut. 3 (2003) 91–101.
- [43] Y. Yao, Y. Xie, B. Zhao, L. Zhou, Y. Shi, Y. Wang, Y. Sheng, H. Zhao, J. Sun, H. Cao, N-dependent ozonation efficiency over nitrogen-containing heterocyclic contaminants: a combined density functional theory study on reaction kinetics and degradation pathways, Chem. Eng. J. 382 (2020) 122708.
- [44] J. Ye, P. Zhou, Y. Chen, H. Ou, J. Liu, C. Li, Q. Li, Degradation of 1H-benzotriazole using ultraviolet activating persulfate: mechanisms, products and toxicological analysis, Chem. Eng. J. 334 (2018) 1493–1501.
- [45] F. Ghanbari, M. Khatebasreh, M. Mahdavianpour, K.Y.A. Lin, Oxidative removal of benzotriazole using peroxymonosulfate/ozone/ultrasound: synergy, optimization, degradation intermediates and utilizing for real wastewater, Chemosphere 244 (2020) 125326.
- [46] Y. Ding, C. Yang, L. Zhu, J. Zhang, Photoelectrochemical activity of liquid phase deposited TiO₂ film for degradation of benzotriazole, J. Hazard. Mater. 175 (2010) 96–103.
- [47] J. Xu, L. Li, C. Guo, Y. Zhang, S. Wang, Removal of benzotriazole from solution by BiOBr photocatalysis under simulated solar irradiation, Chem. Eng. J. 221 (2013) 230–237.
- [48] R. Yin, Y. Chen, S. He, W. Li, L. Zeng, W. Guo, M. Zhu, In situ photoreduction of structural Fe(III) in a metal-organic framework for peroxydisulfate activation and efficient removal of antibiotics in real wastewater, J. Hazard. Mater. 388 (2020) 121996.
- [49] J. Zhang, C. Zhai, W. Zhao, Y. Chen, R. Yin, L. Zeng, M. Zhu, Insight into combining visible-light photocatalysis with transformation of dual metal ions for enhancing peroxymonosulfate activation over dibismuth copper oxide, Chem. Eng. J. 397 (2020) 125310.
- [50] S. He, M. Shen, E. Wu, R. Yin, M. Zhu, L. Zeng, Molecular structure on the detoxification of fluorinated liquid crystal monomers with reactive oxidation species in the photocatalytic process, Environ. Sci. Ecotechnol. 9 (2022) 100141.
- [51] J.M. Wu, Y.G. Sun, W.E. Chang, J.T. Lee, Piezoelectricity induced water splitting and formation of hydroxyl radical from active edge sites of MoS₂ nanoflowers, Nano Energy 46 (2018) 372–382.
- [52] F. Ghanbari, F. Zirrahi, D. Olfati, F. Gohari, A. Hassani, TiO₂ nanoparticles removal by electrocoagulation using iron electrodes: catalytic activity of electrochemical sludge for the degradation of emerging pollutant, J. Mol. Liq. 310 (2020) 113217.